SPADELAB – SPACE DEBRIS LABORATORY OF THE UNIVERSITY OF COIMBRA

N. Peixinho[(1)], R. Gafeira[(1)], L. Vilhena[(2)], A. P. Piedade[(2)], and A. M. Amaro[(2)]

[(1)]*Instituto de Astrofísica e Ciências do Espaço, Observatório Geofísico e Astronómico, Universidade de Coimbra, 3040-004 Coimbra, Portugal, Email: {peixinho, gafeira}@uc.pt*

[(2)]*CEMMPRE, ARISE, Department of Mechanical Engineering, University of Coimbra, 3030-788 Coimbra, Portugal, Email: {luis.vilhena, ana.piedade, ana.amaro}@uc.pt*

ABSTRACT

We present the SpaDeLab – Space Debris Laboratory of the University of Coimbra, a laboratory for the study of space debris analogs born out of an interdisciplinary team combining astronomy, astronomical instrumentation, and surface and mechanical engineering.

Detecting and cataloging space debris (SD) is vital in order to ensure the safety of space assets. However, it is equally vital to identify their composition and estimate their sizes and shapes accurately. The impact energies of SD depend on these parameters. To estimate the sizes of SD, crude assumptions of their reflectivity as a function of the Sun-debris-observer angle, known as the phase-function $\phi(\alpha)$, are used potentially leading to large errors.

Making use of the existing spectroheliograph at the Geophysical and Astronomical Observatory of the University of Coimbra (OGA), with its moving system of mirrors (coelostat), we have redirected the solar light into a second room where an object can be suspended with controlled rotation and axial orientation. Its reflected light is analyzed along a moving arm holding a CCD camera and a photometer equipped with astronomical standard broadband filters (Jonhson BVRI and Sloan g'r'i') to fully measure its brightness (magnitude) phase-function.

With SpaDeLab we are now able to perform a systematic study of different shapes and different compositions of space debris analogs, both from off-the-shelf and from 3D-build objects, with different coatings, different rugosity, and different rotational properties, using the real solar spectrum.

Keywords: Space Debris; Analogs; Photometry; Laboratory; Spectroheliograph.

1. INTRODUCTION

SpaDeLab – Space Debris Laboratory of the University of Coimbra, is an interdisciplinary seed corn project that combines the fields of solar physics, astronomy, surface and mechanical engineering, and materials, addressing both national and international interests in the New Space Economy. With the exponential growth of space activities, the number of SDs is growing exponentially. Keeping highly accurate catalogs is fundamental for all space traffic management and avoiding catastrophic/damaging events on space assets and is becoming increasingly critical. Estimates point to more than 1 million uncatalogued SD in orbit, from 1 cm to 10 cm in size. While cataloging them became a priority, recipes for identifying their composition and adequately estimating their sizes and shapes are of utmost importance, given that their impact energies strongly depend on those parameters. Currently, the sizes of SDs are estimated by making very general and crude assumptions of their reflectivity as a function of the Sun-debris-observer angle, called phase-function $\phi(\alpha)$.

Profiting from the fully functioning Hale-Deslandres spectroheliograph of the Geophysical and Astronomical Observatory of the University of Coimbra [1], recently upgraded, we are setting up a unique facility—the first of its kind in Europe—, combining different disciplines in order to perform a comprehensive study of the reflectivity properties of centimeter-sized SD samples/analogs with various shapes, compositions, coatings, and rugosity using real solar light.

There have been more than 6800 rocket launches into orbit since the beginning of the space age. However, any orbiting body that does not possess a useful purpose or no longer possesses one is technically a piece of SD. Presently, there are about 39 230 objects in orbit being regularly tracked and held in catalogs, of which only around 11 100 are operational satellites. The vast majority is just SD [2, 3, 4]. The large number and concentration of SD represents a serious risk for all space activities and the observation and tracking of SD are mainly done by the Space Surveillance Network (SSN). It is estimated[1] that there are in orbit about 40 500 debris larger than 10 cm, 1 100 000 between 10 cm and 1 cm, and 130 million smaller than 1 cm.

Maintaining a highly accurate catalog is fundamental

[1]ESA's Space Environment Statistics (accessed: 2025-03-20): `https://sdup.esoc.esa.int/discosweb/statistics/`

Proc. 9th European Conference on Space Debris, Bonn, Germany, 1–4 April 2025, published by the ESA Space Debris Office
Editors: S. Lemmens, T. Flohrer & F. Schmitz, (http://conference.sdo.esoc.esa.int, April 2025)

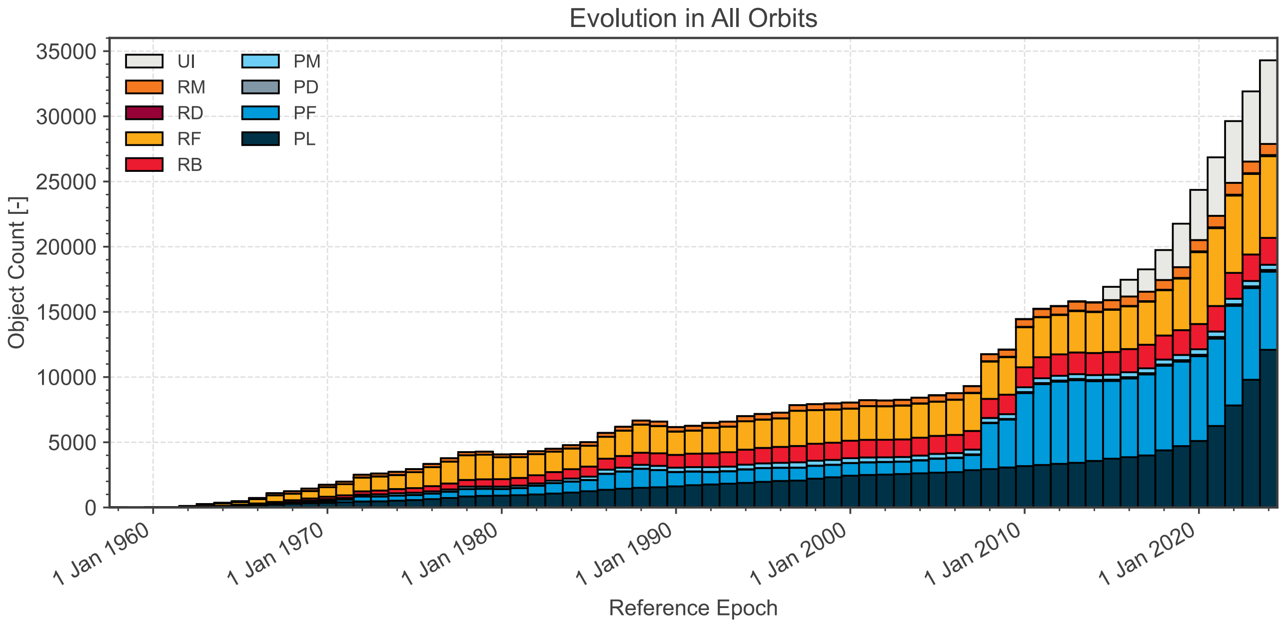

Figure 1. Evolution of the number of objects orbiting the Earth since the dawn of the space age according to ESA's Annual Space Environment Report of 2024 [4]. Objects are classified as being: payloads (PL), payload fragmentation debris (PF), payload debris (PD), payload mission related objects (PM), rocket bodies (RB), rocket fragmentation debris (RF), rocket debris(RD), rocket mission related objects (RM), and objects of unidentified origin (UI).

for space traffic management and avoiding catastrophic events by performing avoidance maneuvers. With the exponential growth of space activities, the number of SD increases drastically and the satellites/spacecrafts are increasingly more vulnerable, as evident from Fig. 1, being the reason why studying space debris plays a vital role in securing future space activities [5, 6].

2. THE PHASE-FUNCTION ISSUE

In astronomy, the apparent magnitude, usually simply called magnitude, is a brightness scale for celestial bodies as seen by an observer. Due to historical reasons, the apparent magnitude, m, or visual magnitude, is measured on a reversed logarithmic scale of brightness (flux) in which a difference of 1 in magnitude corresponds to a brightness factor of 2.5 [7]:

$$m - m_0 = -2.5 \log\left(\frac{F}{F_0}\right) \quad (1)$$

where F is the flux in W/m^2, and the calibration standard being $m_0 = 0$ for a $F_0 = 3.63 \times 10{-}23$ W/m^2. Therefore, the brighter the object, the lower its magnitude. For example, the Sun has a visual magnitude $m_\odot = -26.7$, the star Vega has $+0.03$, being $+6.0$ the naked eye's limiting magnitude.

A very crucial element for the magnitude of an object that only reflects solar light is the Sun-target-observer angle, called phase-angle α (see Fig. 2). The visual magnitude of SD also relates to their ability to reflect the solar light, which depends on many factors like size, distance to the Sun, R, distance to the observer, Δ, phase angle, α, and the albedo/reflectivity, p:

$$m = m_\odot + 5\, log\left(\frac{R\,\Delta}{a^2}\right) - 2.5\, log\left(\frac{p\,A}{a^2}\,\phi(\alpha)\right) \quad (2)$$

where $m_\odot$ is the visual magnitude of the Sun, p is the albedo, A is the cross-section area of the debris, and a is the distance between the Sun and the observer in km, *i.e.*, one astronomical unit, being R and Δ also in km, and $\phi(\alpha)$ is the phase-function [8, 9].

Measuring the magnitude of an SD and knowing the distances to the observer and to the Sun is not hard. As to the albedo, the average value of $p = 0.175$ has been used since 2008 [10] but we need much more measurements and better estimates. If we know also the phase-function then we can estimate the cross-section (size) of the reflecting object (see Eq. 2). However, the phase-angle of an Earth orbiting object varies considerably (see Fig. 2) and while the albedo does not vary with the phase-angle, knowing the brightness dependence with the phase-angle of the orbiting body, the phase-function $\phi(\alpha)$, is crucial to make good size estimates.

Considering ground-based observations when the Sun is θ degrees below the horizon, an object on a circular orbit with altitude h, in the largest angle-variation scenario,

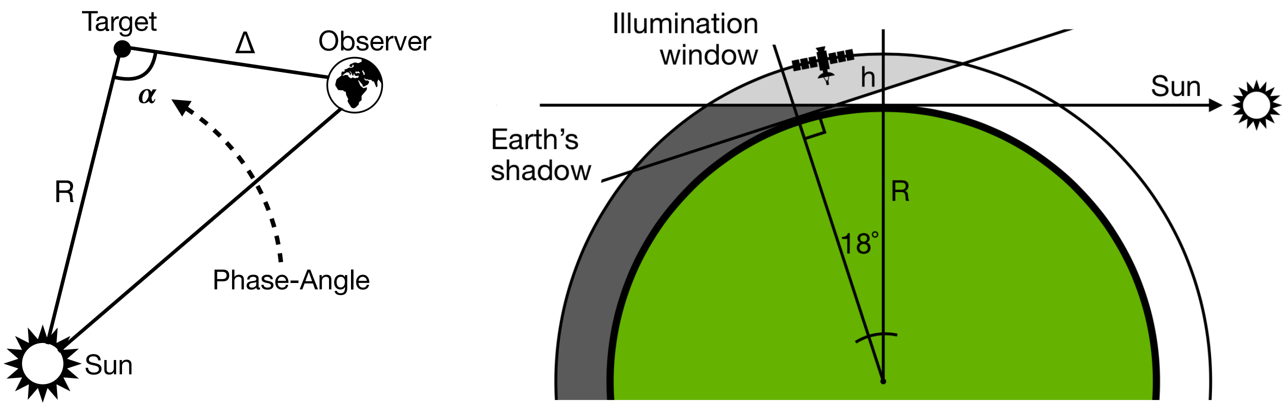

Figure 2. Left: Illustration of the Sun-target-observer angle, called phase-angle ϕ, being R the heliocentric distance, and Δ the geocentric distance. Right: Illustration of the visibility phase-angle range of an orbiting object, at an altitude h above the Earth radius R, reflecting the solar light at the end of the astronomical twilight, i.e., when the Sun is $18°$ below the horizon. Roughly, the maximum phase-angle variation ranges from $\sim 18°$ to $162°$.

can be observed between a maximum and a minimum phase-angle, α, given by:

$$\begin{cases} \alpha_{max} = 180° - \theta \\ \alpha_{min} = \tan^{-1}\left(\frac{R\,(1-\cos\theta)}{\sqrt{2Rh+h^2}-R\,\tan\theta\cos\theta}\right) \end{cases} \quad (3)$$

being R the Earth radius (see Fig. 3). Considering that at the end of the astronomical twilight $\theta = 18°$, assuming a body orbiting Earth at an altitude $h = 500$ km, we will have $\alpha_{max} = 162°$ and $\alpha_{min} = 29.3°$. Note that only orbits higher than 80 km can be observed using ground-based telescopes after astronomical twilight, although that is not a problem for the typical orbits of concern.

The phase-function, however, condenses information from the surface properties of the object together with its illumination and shading conditions. That is, different shapes and different surfaces will generate different phase-functions. For instance, the brightness variation of a light-reflecting object with increasing phase angles is different if that object is a sphere, a cube, or a cylinder and will even be different for different orientations of the cube and the cylinder and for different rugosity of each surface.

In practice, the sizes of SDs are inferred from their magnitudes. However, even maintaining the same distances to the Sun, R, and to the observer, Δ, the brightness greatly depends on the observational phase-angle, α. Being the phase-functions, $\phi(\alpha)$ for the specific materials and shapes largely unknown, a combination of the theoretical phase-functions for the classical diffuse sphere, $\phi_1(\alpha)$, and the specular sphere, $\phi_2(\alpha)$, through a mixing coefficient β in a diffuse-specular model has been used as follows [11] (see Fig. 4):

$$\phi(\alpha) = \beta\,\phi_1(\alpha) + (1-\beta)\,\phi_2(\alpha) \quad (4)$$

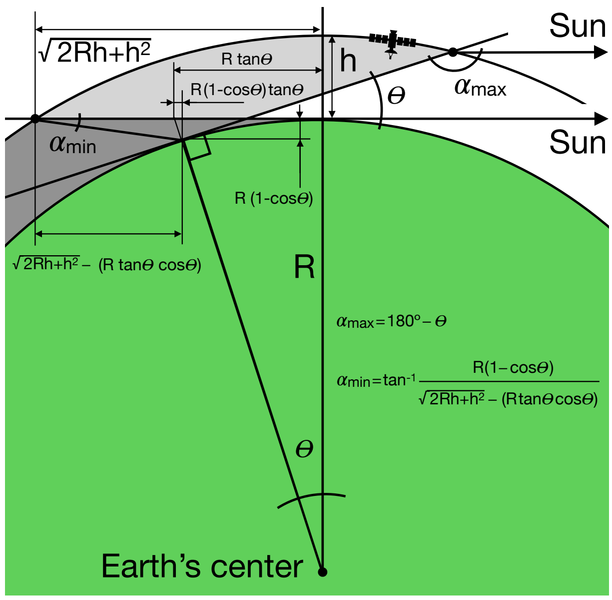

Figure 3. Diagram of α_{max} and α_{min} for an Earth orbiting object as a function of Earth's radius, R, orbiting altitude, h, and solar angle (elevation) below the horizon, θ. The nautical twilight ends at $\theta = 12°$ and the astronomical twilight ends at $\theta = 18°$.

$$\begin{cases} \phi_1(\alpha) = \frac{2}{3\pi^2}\left[(\pi-\alpha)\cos(\alpha)+\sin(\alpha)\right] \\ \phi_2(\alpha) = \frac{1}{4\pi} \end{cases} \quad (5)$$

Further studies have been conducted on the phase-functions of a cylinder, a cube, a rectangular prism, an icosahedron, and a two-sided flat surface [12].

Without proper phase-function correction, the size estimation error can be very large. For example, for largely studied asteroids, it is known that a $+1$ magnitude increase (brightness drop) is easily reached with a $\sim 30°$ increase of α (see Fig. 4, and [13]). Such an error on debris results in 1.6 times under/overestimation of the ra-

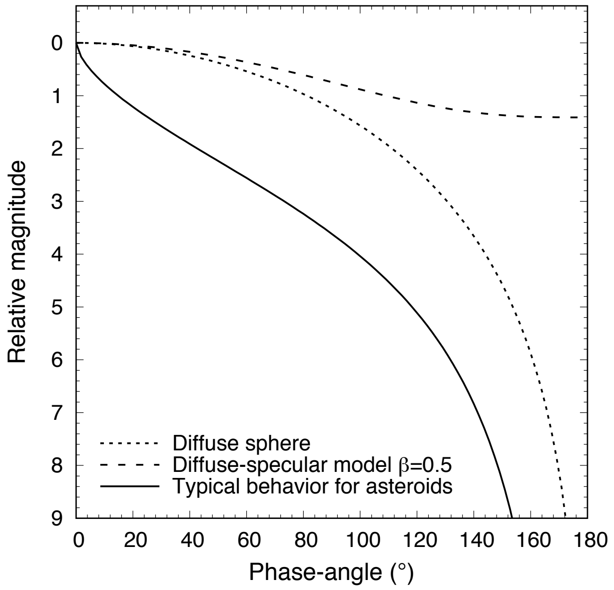

Figure 4. Phase-functions of relative magnitude for a diffuse sphere, a diffuse-specular model with $\beta = 0.5$, and the typical main belt asteroids behavior. The differences are extremely significant.

dius. An apparent 5.0 cm diameter object could have, in fact, 3.2 cm having, therefore, about 4 times less impact energy, and vice-versa. For an orbital height of 500 km, the phase angle ϕ of an SD being observed from the ground varies from about $18°$ to $162°$ (see Fig. 2).

The dynamics of high- and hyper-velocity impacts have been abundantly studied [see 14, for a review]. For the particular case of a metallic SD hitting a metallic satellite, a simple analysis of the penetration of hyper-velocity projectiles [15], considering a spherical impactor, *i.e.* with a length/diameter ratio $L/D = 1$, the total penetration depth, P_d, is approximately given by:

$$P_d = 0.13 \left(\frac{\rho_p}{\rho_t}\right)^{1/3} \left(\frac{E_k}{B_{max}}\right)^{1/3} \tag{6}$$

being, ρ_p the mass density of the projectile, ρ_t mass density of the target, E_k the kinetic energy of the projectile, and B_{max} the maximum target hardness, in kg/mm^2. Since $P_d \propto E_k^{1/3}$, the penetration depth ratio of a spherical metallic object with a given kinetic energy and another with 4 times less kinetic energy (assuming the same mass density for both) is 0.63. This difference shows how important detailed knowledge of the sizes, shapes, and materials of SD is to make a careful assessment of the impact risk on space assets and of their post-impact survival probability.

3. THE LABORATORY'S DESIGN

Knowing the size and shape of an SD does not necessarily tell us much about its composition, mass, and density. Being the full reflectivity spectrum mostly impossible to observe, due to the low brightness of SD, measuring the magnitude differences of an SD observed with different astronomical standard broadband Jonhson BVRI and Sloan g'r'i' filters [see 16, and references therein], called color photometry, is the most promising technique for inferring something about the composition of a detected SD of unknown origin, as has been shown in 2019 [17]. Since virtually all ground-based telescopes are equipped with some astronomical standard broadband filters, we should used them in our laboratory studies.

With SpaDeLab, we will study the phase-curves of a systematic set of simple shapes, with different sizes, colors, compositions, and rugosity, using a varied set of astronomical filters, creating a catalog. Such a catalog will allow for a more precise size estimation of SD, potentially identifying the type of SD, like: metal, polymer, ceramic, etc., allowing therefore a better risk assessment for all space activities.

SpaDeLab will make use of the existing spectroheliograph at the Geophysical and Astronomical Observatory (OGA) of the University of Coimbra. With a moving system of mirrors (coelostat), this facility redirects the solar light into the interior of a building where its spectrum is taken. With a second set of fixed high-quality mirrors we will, when needed, redirect the solar light into another room in the building that will be made dark.

In that room, the beam of solar light will hit a suspended sample of SD, or SD analog, and a moving arm equipped with a CCD camera with standard broadband filters and a photometer will measure the brightness (magnitude) phase-function of the object (see schematics on Fig. 5). By using real solar light instead of artificial light, we will ensure that we are studying the reflectivity properties with the same light spectrum as the one hitting SD in orbit. The only difference being that the light reflected by an SD in orbit will be affected by the atmosphere after the reflection, whereas in the laboratory the solar light will be affected by the atmosphere before being reflected by the SD analog, outcome being identical.

4. FUTURE WORK

Once the laboratory room is up and running, we will carefully measure the phase-angle brightness drop in our dark room. The target, the SD analog, is fixed and illuminated by a collimated beam of solar light, redirected from the coelostat. The reflected light is measured in increasing phase-angles, from $\sim 5°$ to $\sim 175°$, both by a photometer and a CCD imager, measuring the reflectivity for each angle in different filters.

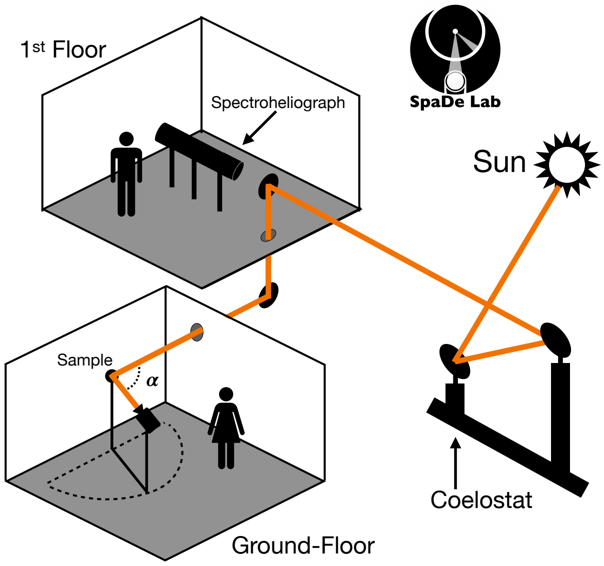

Figure 5. Schematics of SpaDeLab's laboratory in the spectroheliograph building of the Geophysical and Astronomical Observatory of the University of Coimbra.

A second photometer will measure the direct solar light for calibration from any solar brightness alteration. The background noise of the dark room, where some dispersed light may exist, will be measured for every angle and subtracted. Standard CCD photometric measurements will be performed and the results compared with those of the photometer. The phase-curves derived from the CCD imaging and from the photometer must be equal.

The first set of samples to be analyzed will be spheres, cubes, and cylinders, of 3 cm, 2 cm, and 1 cm, polished and with increasing rugosity, copper coated, aluminum coated and titanium coated. Other SD analogs, with different degrees of weathering obtained from the "ESA Space Debris Office" will be studied. Upon the analysis of this first set, we will move on to the more complex substances of 3D-printed ceramics and polymers, as well as L-shapes, T-shapes, and other expected shapes of SD according to hyper-velocity breakup experiments [18]. From the phase-curves obtained for each target, with its different properties, we expect to quantify and catalog the effects of different sizes, shapes, substances, coatings, and rugosity, on each standard filter, together with the corresponding photometric colors.

ACKNOWLEDGMENTS

This project has received funding from Santander Portugal Foundation under the 5th Edition of "Seed Projects for Interdisciplinary Research" call, promoted by the University of Coimbra. N.P. and R.G. acknowledge funding by Fundação para a Ciência e a Tecnologia (FCT) through the research grants UIDB/04434/2020 (DOI: 10.54499/UIDB/04434/2020) and UIDP/04434/2020 (DOI: 10.54499/UIDP/04434/2020). L.V., A.P.P, and A.M.M.'s research is sponsored by national funds through Fundação para a Ciência e a Tecnologia (FCT), under projects UID/00285 – Centre for Mechanical Engineering, Materials and Processes and LA/P/0112/2020.

REFERENCES

1. Lourenço, A., Carvalho, S., Barata, T., Garcia, A., Carrasco, V., Peixinho, N. 2019. Solar observations at the Coimbra Astronomical Observatory. Open Astronomy 28, 165–179. doi:10.1515/astro-2019-0015
2. Bonnal, C., McKnight, D. S. 2017. IAA Situation Report on Space Debris – 2016. Paris, International Academy of Astronautics, May 2017.
3. NASA 2021. NASA's Efforts to Mitigate the Risks Posed by Orbital Debris. Report No. IG-21-011, January 2021.
4. ESA, Space Debris Office 2024. ESA's Annual Space Environment Report. Reference: GEN-DB-LOG-00288-OPS-SD, 19 July 2024.
5. Kessler, D. J., Cour-Palais, B. G. 1978. Collision frequency of artificial satellites: The creation of a debris belt. Journal of Geophysical Research 83, 2637–2646. doi:10.1029/JA083iA06p02637
6. NASA 2023. NASA Spacecraft Conjunction Assessment and Collision Avoidance Best Practices Handbook. NASA/SP-20230002470 Rev 1, February 2023.
7. Pogson, N. 1856. Magnitudes of Thirty-six of the Minor Planets for the first day of each month of the year 1857. Monthly Notices of the Royal Astronomical Society 17, 12–15. doi:10.1093/mnras/17.1.12
8. Russell, H. N. 1916. On the Albedo of the Planets and Their Satellites. The Astrophysical Journal 43, 173–196. doi:10.1086/142244
9. Bowell, E., Hapke, B., Domingue, D., Lumme, K., Peltoniemi, J., Harris, A. W. 1989. Application of photometric models to asteroids. Asteroids II, 524–556.
10. Mulrooney, M., Matney, M., Hejduk, M., Barker, E. 2008. An Investigation of Global Albedo Values. Advanced Maui Optical and Space Surveillance Technologies Conference 2008 Conference Proceedings
11. Hejduk, M. 2011. Specular and Diffuse Components in Spherical Satellite Photometric Modeling. Advanced Maui Optical and Space Surveillance Technologies Conference 2011 Conference Proceedings.
12. Hejduk, M., Cowardin, H., Stansbery, E. 2012. Satellite Material Type and Phase Function Determination in Support of Orbital Debris Size Estimation. Advanced Maui Optical and Space Surveillance Technologies Conference 2012 Conference Proceedings.
13. Shevchenko, V. G. and 8 colleagues 2019. Phase integral of asteroids. Astronomy and Astrophysics 626. doi:10.1051/0004-6361/201935588
14. Anderson Jr., Ch. E. 2017. Analytical models for penetration mechanics: A Review. International Journal of Impact Engineering 108, 3–126. doi:10.1016/j.ijimpeng.2017.03.018

15. Christman, D. R., Gehring, J. W. 1966. Analysis of High-Velocity Projectile Penetration Mechanics. Journal of Applied Physics 37, 1579–1587. doi:10.1063/1.1708570

16. Bessell, M. S. 2005. Standard Photometric Systems. Annual Review of Astronomy and Astrophysics 43, 293–336. doi:10.1146/annurev.astro.41.082801.100251

17. Zigo, M., Silha, J., Krajčovič, S. 2019. BVRI Photometry of Space Debris Objects at the Astronomical and Geophysical Observatory in Modra. Advanced Maui Optical and Space Surveillance Technologies 2019 Conference Proceedings.

18. Cowardin, H.,Anz-Meador, Ph., Murray, J., Liou, J.-C., Christiansen, E., Sorge, M., Fitz-Coy, N., Huynh, T. 2019. Updates to the DebriSat Project in Support of Improving Breakup Models and Orbital Debris Risk Assessments. Proceedings of the 2019 15th Hypervelocity Impact Symposium. doi:10.1115/HVIS2019-066